A new continuum approach for nonlinear kinetic simulation and transport analysis

Zongliang Dai, Yingfeng Xu, Lei Ye, Xiaotao Xiao, and Shaojie Wang

Citation: Physics of Plasmas **22**, 022301 (2015); doi: 10.1063/1.4906051
View online: http://dx.doi.org/10.1063/1.4906051
View Table of Contents: http://scitation.aip.org/content/aip/journal/pop/22/2?ver=pdfcov
Published by the AIP Publishing

A new continuum approach for nonlinear kinetic simulation and transport analysis

Zongliang Dai,[1,a)] Yingfeng Xu,[2] Lei Ye,[2] Xiaotao Xiao,[2] and Shaojie Wang[1]
[1]*Department of Modern Physics, University of Science and Technology of China, Hefei 230026, China*
[2]*Institute of Plasma Physics, Chinese Academy of Science, Hefei 230031, China*

(Received 4 November 2014; accepted 5 January 2015; published online 2 February 2015)

A numerical code based on the I-transform approach is developed to solve the nonlinear Vlasov equation and carry out the transport analysis. The numerical results given by the I-transform approach agree with the conservative semi-Lagrangian approach in the Landau damping case and the bump-on-tail instability case. The diffusivities induced by the random fields and the quasilinear transport are also successfully demonstrated by using the new approach. It is found that the nonlinear transport in the one-dimensional Langmuir turbulence cannot be well-described by a simple diffusion model, due to the strong particle trapping at the nonlinear stage. © *2015 AIP Publishing LLC*.
[http://dx.doi.org/10.1063/1.4906051]

I. INTRODUCTION

Plasma transport is an important and difficult problem in tokamak physics. The neoclassical transport theory[1,2] and the quasilinear transport theory (QLT)[3] have made great progress, but still the anomalous transport cannot be fully explained.[4] Nowadays, it is believed that the nonlinear micro-turbulence leads to the anomalous transport. The turbulence transport can be investigated by solving the nonlinear Vlasov equation.

Due to the nonlinear coupling between the particle motion and the fields, theoretical analysis is difficult. Numerical simulations now play a major role in the investigation of the low-frequency plasma turbulence.[5] Two classes of numerical methods are widely used in the gyrokinetic simulation: the particle-in-cell (PIC) method and the continuum method. The PIC method, which is the most widely used numerical method, calculates the evolution of the system by following the orbits of a huge number of particles in the phase space. However, the sampling noise in the course of a simulation by the PIC method makes it difficult to precisely describe the low density regions.[6] When the random walk model is used, the diffusivity can be directly obtained by computing the mean square displacement (MSD).[7] Another numerical method is the continuum method, which describes the plasma by the distribution function F in the phase space on a fixed grid. There are two approaches, the Eulerian approach and the semi-Lagrangian (SL) approach in the continuum method. The Eulerian approach solves the Vlasov equation by using the usual numerical scheme such as the finite difference method or the finite element method. The high order finite difference schemes can reduce the numerical dissipation, but it will cause unphysical oscillations. On the other hand, if the explicit time integration is applied, the maximum time step will be limited by the Courant-Friedrichs-Lewy (CFL) stability condition.[5] In the semi-Lagrangian approach, the value of F at grid points is obtained by interpolation at the foot of the orbit. The CFL restriction is removed in the SL approach. The high order interpolation scheme is less dissipative; however, it can also lead to unphysical oscillations. Time operator splitting method can be applied to avoid the high dimensional interpolation, but the conservation laws are not well-satisfied when using the splitting methods.[8] Note that in the continuum approach, it is difficult to explicitly compute the transport coefficients.

Recently, a new formulation, the I-transform (IT) approach,[9–14] of the nonlinear gyrokinetic Vlasov equation has been proposed, which decouples the stochastic motion from the regular motion by using the Lie-transform perturbation method.[15,16] The Vlasov equation has been formulated in the Fokker-Planck form, which explicitly represents the diffusion and convection in the phase space. The prediction of diffusivity by the I-transform has successfully demonstrated the result of the QLT.[10] In this work, a continuum code based on the I-transform approach is developed to simulate the one dimensional Vlasov-Poisson (VP) system. Two numerical examples are given to verify the new code; for the transport analysis, the diffusivities explicitly computed by the new code are compared with the results computed in different ways.

The remaining part of this paper is organized as follows. In Sec. II, the basic equations and two numerical approaches of the I-transform method are presented. In Sec. III, two numerical tests are given to validate the new approach. In Sec. IV, the diffusion coefficients are computed in different perturbation fields with different methods. In Sec. V, the main results are summarized and discussed.

II. BASIC EQUATIONS AND NUMERICAL APPROACHES

A. One-dimensional VP system and the I-transform approach

The one-dimensional VP equations are written as

$$(\partial_t + v\partial_x + \delta E\partial_v)F = 0, \tag{1a}$$

a)E-mail: liangliang1223@gmail.com

$$\partial_x \delta E = \int_{-\infty}^{\infty} F \mathrm{d}v - 1, \tag{1b}$$

where $F(x, v, t)$ is the electron distribution function and $\delta E(x, t)$ is the electric field. In this paper, time is normalized to the inverse electron plasma frequency ω_{pe}^{-1}, space is normalized to the Debye length λ_D, and velocity is normalized to the electron thermal speed $V_{T_e} = \lambda_D \omega_{pe}$. Ions are assumed to be static, and their only role is to provide a uniform, neutralizing background.[17]

The characteristic lines of Eq. (1a) are equivalent to the trajectories of particles, which can be described by the following equations of motion:

$$\dot{x} = v, \tag{2a}$$

$$\dot{v} = \delta E. \tag{2b}$$

The distribution function $F(x_i, v_j, t_{n+1}) = F(x_i', v_j', t_n)$. Here, (x_i', v_j') is the phase-space coordinate of a particle at t_n, and (x_i, v_j) is the coordinate at t_{n+1} computed by Eq. (2). Either the two dimensional interpolation or the operator splitting method can be used to calculate $F(x_i', v_j', t_n)$ in the semi-Lagrangian approach. The I-transform approach transforms the perturbation into the Lie transform generating fields, which is similar to the modern gyrokinetics for decoupling the fast gyromotion. The new approach does not evolve the real system, which shall be referred to as "P0," but evolves a simpler image system, which shall be referred to as "P1."

The fundamental one-form Γ and the extended Hamiltonian $\mathcal{H}$ in the four-dimensional extended phase space $\boldsymbol{Z} = (v, -w, x, t)$ is expressed as

$$\Gamma \equiv \Gamma_i \mathrm{d}Z^i = v\mathrm{d}x - w\mathrm{d}t - \mathcal{H}\mathrm{d}\tau, \tag{3a}$$

$$\mathcal{H} \equiv \mathcal{H}_0 + \mathcal{H}_1 = \frac{1}{2}v^2 - w + \delta\phi, \tag{3b}$$

with w the total energy of the particle, τ the independent parameter, $\delta\phi$ the electrostatic potential perturbation, and $\delta E = -\partial_x \delta\phi$ the electrostatic field perturbation. Equation (1a) can be written in the form

$$\{F, \mathcal{H}\} = 0. \tag{4}$$

The gauge function $\mathcal{S}_n$'s is used to remove the perturbation dependence of the extended Lagrangian, so that the equation of motion in P1 is unperturbed, which are simply

$$\dot{x} = v, \tag{5a}$$

$$\dot{v} = 0. \tag{5b}$$

The transformed Lagrangian is formally same as the unperturbed one, that is, $\bar{\Gamma}_i = \Gamma_{0i}$, $\bar{\mathcal{H}} = \mathcal{H}_0$, $\bar{\Gamma}_1 = \bar{\Gamma}_2 = 0$, $\bar{\mathcal{H}}_1 = \bar{\mathcal{H}}_2 = 0$.[10]

Then, we can obtain expressions of the gauge functions $\mathcal{S}_1$ and $\mathcal{S}_2$ by the Lie-transform perturbation method

$$\{\mathcal{S}_1, \mathcal{H}_0\} = \mathcal{H}_1, \tag{6a}$$

$$\{\mathcal{S}_2, \mathcal{H}_0\} = -\frac{1}{2}\mathcal{G}_1^i \partial_i \mathcal{H}_1, \tag{6b}$$

where $\{,\}$ is the Poisson bracket, and the generating vector fields $\mathcal{G}_n$'s can be calculated by

$$\mathcal{G}_n^i = \{\mathcal{S}_n, Z^i\}. \tag{7}$$

The transformations of the variables between P0 and P1 are explicitly written as

$$\bar{Z}^i = Z^i + \mathcal{G}_1^i + \mathcal{G}_2^i + \frac{1}{2}\mathcal{G}_1^j \partial_j \mathcal{G}_1^i, \tag{8a}$$

$$Z^i = \bar{Z}^i - \mathcal{G}_1^i - \mathcal{G}_2^i + \frac{1}{2}\mathcal{G}_1^j \partial_j \mathcal{G}_1^i, \tag{8b}$$

with $\bar{\boldsymbol{Z}}$ the coordinate in P1, $\boldsymbol{Z}$ the coordinate in P0. The governing equations of the I-transform approach are

$$\bar{F} = F - \mathcal{G}_1^i \partial_i F - \mathcal{G}_2^i \partial_i F + \frac{1}{2}\mathcal{G}_1^j \partial_j \mathcal{G}_1^i \partial_i F, \tag{9a}$$

$$\partial_t \bar{F} + v\partial_x \bar{F} = 0, \tag{9b}$$

$$\partial_t \mathcal{S}_1 + v\partial_x \mathcal{S}_1 = \delta\phi, \tag{9c}$$

$$\partial_t \mathcal{S}_2 + v\partial_x \mathcal{S}_2 = \frac{1}{2}\mathcal{G}_1^x \delta E, \tag{9d}$$

$$\mathcal{G}_n^x = -\partial_v \mathcal{S}_n, \tag{9e}$$

$$\mathcal{G}_n^v = \partial_x \mathcal{S}_n, \tag{9f}$$

$$F = \bar{F} + \mathcal{G}_1^i \partial_i \bar{F} + \mathcal{G}_2^i \partial_i \bar{F} + \frac{1}{2}\mathcal{G}_1^j \partial_j \mathcal{G}_1^i \partial_i \bar{F}, \tag{9g}$$

with $\bar{F}$ the distribution function in P1 and F the real distribution function in P0.

B. Transport analysis, the single-step transform

The solution of Eq. (9c) can be computed by using the characteristic method,

$$\mathcal{S}(x_i, v_j, t_{n+1}) = \mathcal{S}(x_{0i}, v_{0j}, t_n) + \int_{t_n}^{t_{n+1}} \delta\phi(x(t'), v(t'), t')\mathrm{d}t', \tag{10}$$

with $x(t')$, $v(t')$ computed by Eq. (5). Equations (9b) and (9d) are also solved in a similar way. Note that the explicit time-dependence of $\delta\phi(x, v, t)$ can be treated by using the prediction-correction algorithm, when (t_n, t_{n+1}) is set as the minimal computation time step.

For the convenience of simulation, the initial values of gauge functions are $\mathcal{S}_n(t_0) = 0$, which means that the initial transformation is the identical transformation, the initial state of P1 is equal to the state of P0 and the transformed distribution function is also equal to the untransformed one, $\bar{F}(t_0) = F(t_0)$. After that, $\bar{F}$ of P1 is evolved according Eq. (9b), $\bar{F}(x, v, t_0 + t) = \bar{F}(x - vt_0, v, t_0) = F(x - vt_0, v, t_0)$. $\mathcal{S}$, $\mathcal{G}$, $\delta\phi$, F are evolved by solving Eqs. (9c)–(9g) and (1b). The initial transformation is used only one time, so that the above solution based on the I-transform approach is called a single-step transformation (SST). The SST is schematically shown in Fig. 1.

If the perturbation field is random or the deviation between the perturbed and the unperturbed system is weak, the transport equation and the turbulence scattering term can

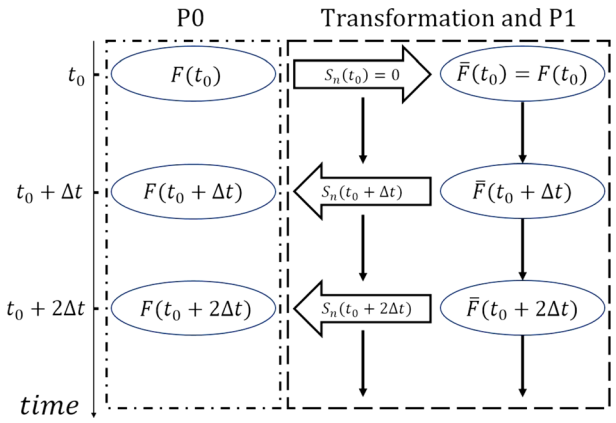

FIG. 1. F is the real distribution function in P0 and $\bar{F}$ is the transformed distribution function in P1. The evolution of P1 is simpler than the one of P0.

be found by using the SST.[12,14] Note that $\mathcal{G}_n$'s are incompressible flows in phase space[10]

$$\partial_i \mathcal{G}_n^i = 0. \tag{11}$$

Substituting Eq. (11) into Eq. (9g), we have

$$F = \bar{F} + \partial_i \left(\mathcal{G}_1^i + \mathcal{G}_2^i + \frac{1}{2} \mathcal{G}_1^i \mathcal{G}_1^j \partial_j \right) \bar{F}. \tag{12}$$

Note that

$$\bar{F}(x + v\tau, v, t + \tau) = \bar{F}(x, v, t) = F(x, v, t). \tag{13}$$

Using Eqs. (12) and (13), one finds

$$\begin{aligned} &\left(\frac{\mathrm{d}}{\mathrm{d}\tau} \right)_0 F(x,v,t) \\ &= \frac{F(x+v\tau, v, t+\tau) - F(x,v,t)}{\tau} \\ &= -\partial_i \left[a_{\mathcal{T}}^i (x+v\tau, v, t) - \frac{1}{2} d_{\mathcal{T}}^{ij} (x+v\tau, v, t) \partial_j \right] F(x,v,t). \end{aligned} \tag{14}$$

The phase space convection vector $\boldsymbol{a}_{\mathcal{T}}$ and the symmetric diffusion tensor $\boldsymbol{d}_{\mathcal{T}}$ are given by

$$a_{\mathcal{T}}^i \equiv -\frac{\mathcal{G}_{1,\tau}^i}{\tau} - \frac{\mathcal{G}_{2,\tau}^i}{\tau}, \tag{15a}$$

$$d_{\mathcal{T}}^{ij} \equiv \frac{\mathcal{G}_{1,\tau}^i \mathcal{G}_{1,\tau}^j}{\tau}. \tag{15b}$$

It has been proved that the diffusivity calculated by the turbulence scattering term agree with the prediction of the QLT.[10]

C. Simulation scheme, the multiple-step transform

Since the I-transform approach is based on the Lie transform perturbation method, if a large deviation between the real orbit and the unperturbed orbit occurs, the results will not be accurate for a SST. Therefore, it is not accurate to predict the long-time behavior of a system with a strong perturbation by applying a SST. To avoid this secular problem, the multiple-step transform (MST) is proposed as a simulation tool,[14] which is adopted in this work.

Note that the initial push-forward transformation can be applied at any time, so that the transformation and P1 system can be redefined at any time in the simulation. In other words, the SST can be used in a step by step way: $F(x, v, t_n)$ is evolved for only one time step Δt by using a SST to compute $F(x, v, t_{n+1})$. This is called a MST. Fig. 2 shows the physical picture of the SST and the MST to calculate the particle orbit, which is similar to the computation of the distribution function.

III. NUMERICAL RESULTS

In this section, the numerical results of the I-transform approach by using the MST will be shown. To verify the new code, the code based on the operator splitting method[18] and the conservative semi-Lagrangian approach[19] is used as a benchmark in the following numerical examples.

The VP model preserves some physical quantities with time. First of all, it preserves the total particle number N,

$$N(t) = \int\int F(x, v, t) \mathrm{d}x \mathrm{d}v. \tag{16}$$

The total energy is also constant in time,

$$\mathcal{E}(t) = \mathcal{E}_k(t) + \mathcal{E}_e(t) = \int\int \frac{1}{2} v^2 F(x, v, t) \mathrm{d}x \mathrm{d}v + \int \frac{1}{2} E^2(x, t) \mathrm{d}x, \tag{17}$$

where $\mathcal{E}_e$ and $\mathcal{E}_k$ denote the electric and kinetic energy, respectively. The relative error of the particle number ΔN and the total energy $\Delta \mathcal{E}$ are defined as

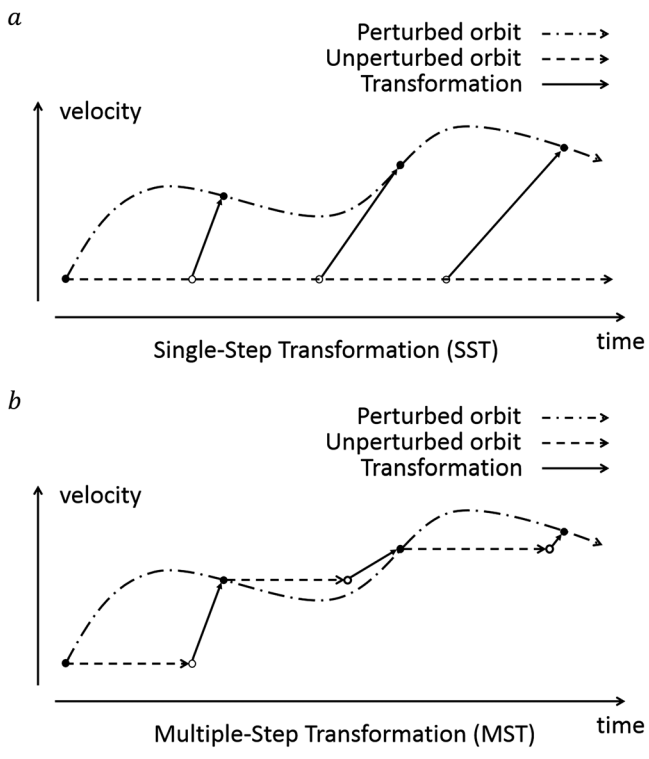

FIG. 2. The SST and the MST to compute the particle orbit.

$$\Delta N(t) = \frac{N(t) - N(0)}{N(0)}, \tag{18a}$$

$$\Delta \mathcal{E}(t) = \frac{\mathcal{E}(t) - \mathcal{E}(0)}{\mathcal{E}(0)}. \tag{18b}$$

The first test is the Landau damping. The initial condition associated with the VP model is

$$F(t=0) = \frac{1}{\sqrt{2\pi}} \exp\left\{-\frac{v^2}{2}\right\}(1 + \alpha \cos kx),$$
$$x \in [0, L], \quad v \in [-6, 6], \tag{19}$$

where $L = 2\pi/k$. The grid numbers of phase space are $(N_x, N_v) = (129, 513)$. The parameters (k, α) can be chosen as (0.5, 0.05) to simulate the linear Landau damping, and (0.5, 0.04) to simulate the nonlinear case.[20] In the linear case, the time step $\Delta t = 0.1$ and the number of iterations $T = 600$; in the nonlinear case $(\Delta t, T) = (0.1, 1000)$. After that, the parameters are chosen as $(k, \alpha; \Delta t, T) = (0.5, 0.8; 0.01, 10\,000)$ to test the application of the new code in the strong perturbation case.

From Fig. 3, one concludes that the results by the I-transform code agree well with the results by the semi-Lagrangian code. The conservations of particle number and total energy are similar for both codes. In Fig. 4, we also plot the ensemble averaged distribution functions for the linear and the nonlinear Landau damping cases, with the ensemble average defined as

$$\langle F \rangle = \frac{1}{L} \int_L F \mathrm{d}x. \tag{20}$$

It is clear to see that the negative gradient slop in the ensemble averaged distribution function appears in the nonlinear Landau damping, but it does not appear in the linear case.

Although the I-transform approach is based on the perturbative method, the strong perturbation case can also be treated, as is shown in Figs. 3(3a), 3(3b), and 3(3c). Actually, if the time step is kept small enough, the deviation between the perturbed system and the unperturbed one can also be kept small enough, which makes the MST method applicable.

The second test is the Bump-on-tail (BOT) instability. The initial distribution function is

$$F = \langle F \rangle + \tilde{F}, \quad x \in \left[0, \frac{2\pi}{k_{min}}\right], \quad v \in [-15, 15],$$
$$\langle F \rangle = \frac{0.7}{\sqrt{\pi}} \exp\left\{-\left(\frac{v+5}{1}\right)^2\right\} + \frac{0.3}{5\sqrt{\pi}} \exp\left\{-\left(\frac{v+5-5}{5}\right)^2\right\},$$
$$\tilde{F} = \frac{\delta}{\sqrt{100}} \sum_{i=1}^{100} \cos(k_i x - \varphi_i), \tag{21}$$

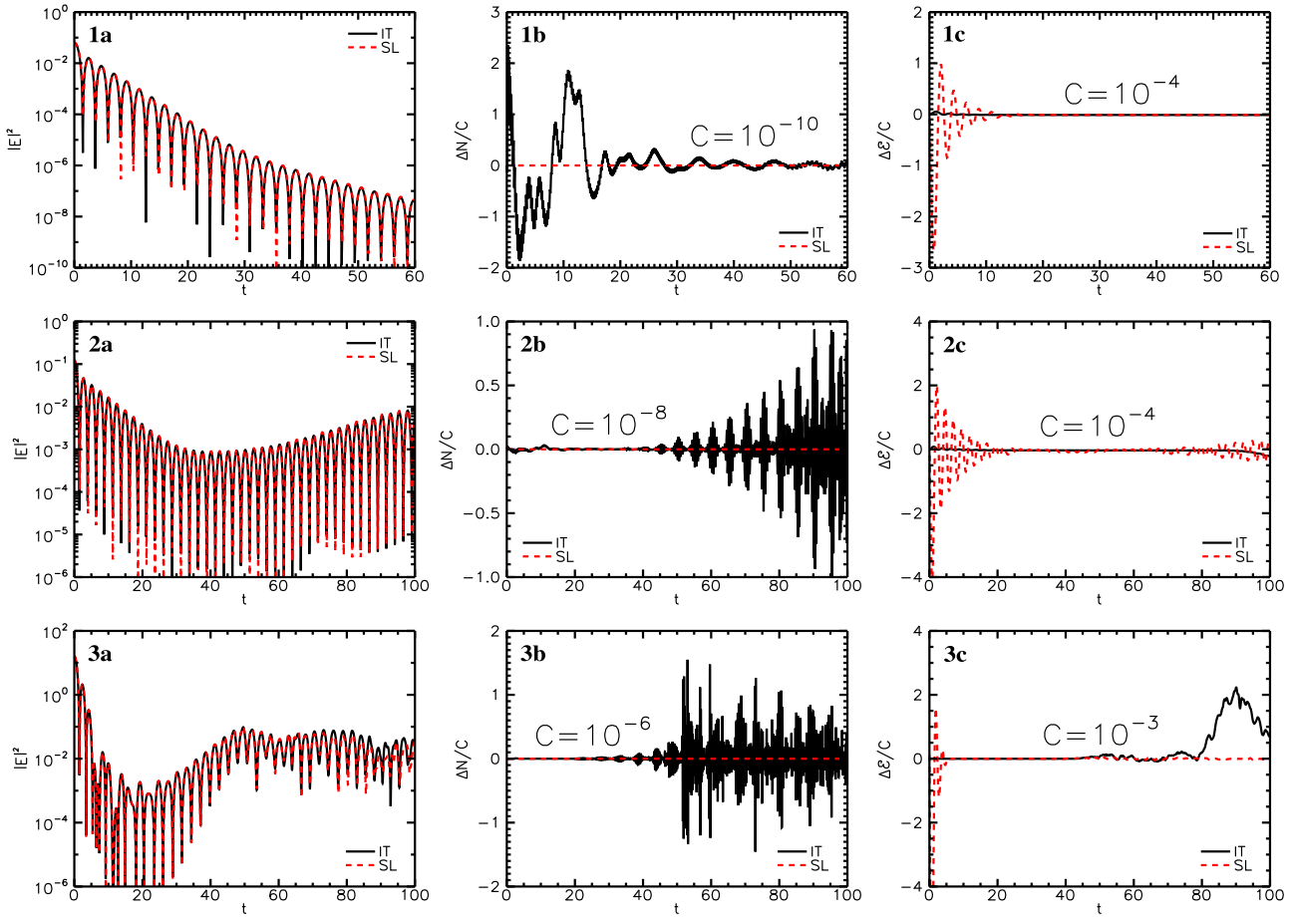

FIG. 3. Numerical results of the Landau damping. (1) The linear Landau damping case $(k, \alpha; \Delta t, T) = (0.5, 0.05; 0.1, 600)$. (2) The nonlinear Landau damping case $(k, \alpha; \Delta t, T) = (0.4, 0.05; 0.1, 1000)$. (3) The nonlinear Landau damping for large perturbation $(k, \alpha; \Delta t, T) = (0.5, 0.8; 0.10, 10000)$. (a) Time history of the electric energy, which are normalized to C. (b) Relative error of the particle number, which are normalized to C. (c) Relative error of the total energy. IT: Results of the I-transform approach. SL: Results of the semi-Lagrangian approach.

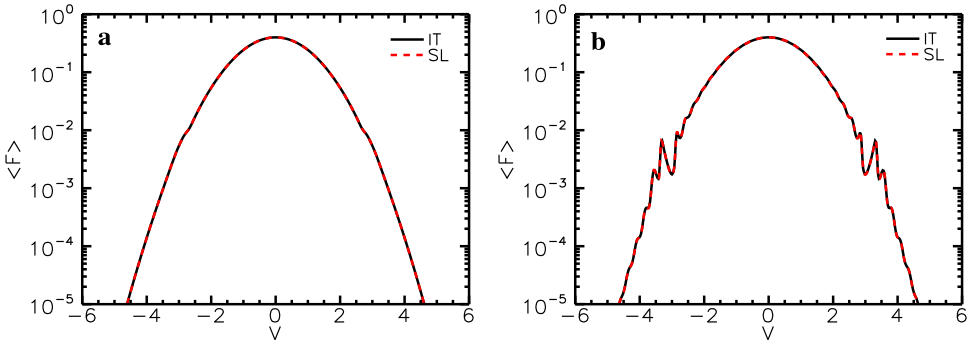

FIG. 4. Ensemble averaged distribution function at $t = 60$. (a) Linear Landau damping case. (b) Nonlinear Landau damping case.

with $\tilde{F}$ the initial perturbation, $\delta = 10^{-4}$, $k_i = ik_{min}$, $k_{min} = 0.01$, the grid number of phase space $(N_x, N_v) = (1025, 1025)$, time step $\Delta t = 0.01$, and the number of iterations $T = 30\,000$. From Figs. 5 and 6, it is clearly seen that both of the codes predict the same electric field and ensemble averaged distribution function. The electric field and the ensemble averaged distribution function will be used in Sec. IV for discussing the transport analysis.

The results show good agreement between the two codes in different numerical cases, which clearly demonstrates that the I-transform approach is valid for solving the nonlinear Vlasov equation.

IV. TRANSPORT ANALYSIS

In this section, the diffusion processes in the velocity space caused by different perturbed electric fields are discussed. The transport process in the velocity space can be described by

$$\partial_t \langle f \rangle + \partial_v \gamma = 0 \tag{22}$$

with γ the flux in the velocity space, which will be computed in different ways and compared with each other. The first method for calculating the flux is to integrate Eq. (22) directly

$$\gamma_I = -\int_{-\infty}^{v} \frac{\langle f(v', t_f)\rangle - \langle f(v', t_i)\rangle}{t_f - t_i} \mathrm{d}v'. \tag{23}$$

Calculating the diffusivity D is another way to obtain the flux. In the PIC method, the diffusion coefficient D can be obtained by computing the MSD.

$$D_{MSD} = \frac{1}{2}\left\langle \frac{(v - \langle v\rangle)^2}{t_f - t_i} \right\rangle, \tag{24a}$$

$$\gamma_{MSD} = D_{MSD}\partial_v \langle f\rangle. \tag{24b}$$

However, it is difficult for a traditional continuum code to explicitly compute the diffusivity. In the I-transform approach, the transport coefficients are explicitly given by Eq. (15). Using the SST, one can compute the flux and the diffusivity through

$$D_{SST} = \frac{1}{2}\left\langle \frac{\mathcal{G}_1^v \mathcal{G}_1^v}{t_f - t_i} \right\rangle, \tag{25a}$$

$$\gamma_{SST} = D_{SST}\partial_v \langle f\rangle. \tag{25b}$$

In the following part of this section, transport fluxes and particle orbits computed in different ways are compared with each other.

First, the diffusion of the test particle in a pseudo random phase field is computed. The perturbed field is expressed in the following form:

$$\phi(x, t) = \sum_{i=1}^{100} \delta_i \cos(k_i x + \varphi_{ran,i}), \tag{26}$$

with $\delta_i = 0.1 \exp\{-16(k_i - 0.5)^2\}$, $k_i = 0.01$, and $\varphi_{ran,i}$ the random number. The phase space grid number $(N_x, N_v) = (513, 513)$, time step $\Delta t = 0.0001$, and the number of iterations $T = 10\,000$. The value of $\varphi_{ran,i}$ will be reset per $\tau_0 = 100\Delta t$. The distribution function of the test particle is

$$F(x, v, 0) = \frac{1}{\sqrt{2\pi}} \exp\left\{-\frac{v^2}{2}\right\}. \tag{27}$$

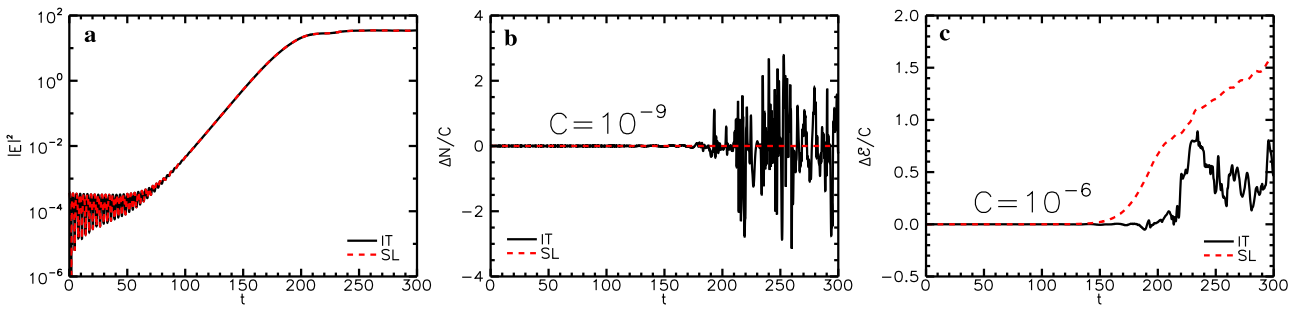

FIG. 5. Numerical results of the BOT instability. (a) Time history of the electric energy. (b) Relative error of the particle number, which is normalized to C. (c) Relative error of the total energy, which is normalized to C.

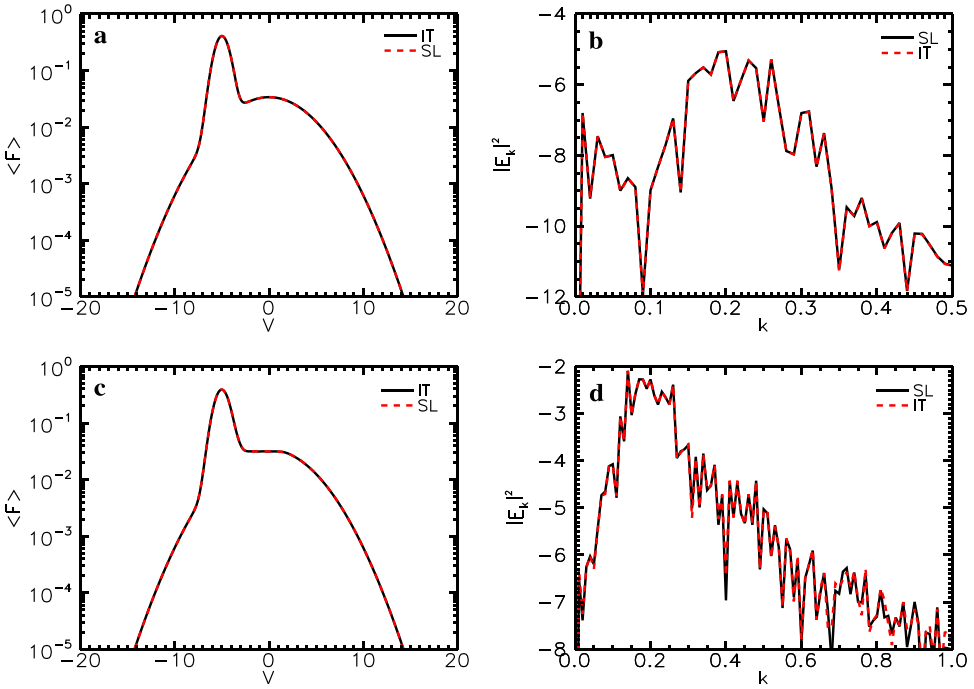

FIG. 6. (a) and (b) The ensemble averaged distribution function and the energy spectrum of the electric field at linear stage ($t = 120$). (c) and (d) The ensemble averaged distribution function and the energy spectrum of the electric field at nonlinear stage ($t = 300$).

It can be seen from Fig. 7(a) that the diffusivity in the velocity space caused by the random phase field is well described by the turbulence scattering term. On a short time scale, $\mathcal{G}_1^v\mathcal{G}_1^v$ is proportional t^2, as is shown in Figs. 7(b) and 7(c). However, on the time scale longer than the random time scale, $\mathcal{G}_1^v\mathcal{G}_1^v/t$ tends to a constant, and the diffusion in velocity space can be well described with this constant.

Next, the quasilinear ($t \in [100, 150]$) and nonlinear ($t \in [250, 300]$) diffusivity of the Langmuir turbulence excited by the BOT instability will be computed by using the self-consistent fields computed in Sec. III. It can be seen from Fig. 8 that the quasilinear diffusion computed in different ways agree well with each other. However, the nonlinear diffusion obtained by different ways does not give the same results, which is shown in Fig. 9.

To analyse the reason of the disagreement at the nonlinear stage, the particle orbits in the nonlinear fields are computed by using both the 2nd-order Runge-Kutta method and the SST. The process of evolving particle orbits is the same as the process of evolving the distribution function. From Fig. 10, it can be seen that the orbits computed by the SST do not agree with the results by the traditional Runge-Kutta method at the nonlinear stage. The orbit analysis at the linear stage is shown in Fig. 11, which indicates that the SST accurately predicts the quasilinear behaviour.

Note that the large error of the SST (Fig. 10(c)) occurs in the plateau region of the ensemble averaged distribution function at the nonlinear stage, which implies that the effects of nonlinear field on the particles in the plateau region (Fig. 6(c)) are quite different. To figure out the difference in this region, the phase velocity $V_p(k, t)$ of different wave number k is diagnosed

$$V_p(k,t) = -\frac{1}{k}\frac{\mathrm{d}}{\mathrm{d}t}\arg(E_k) \approx -\frac{1}{k}\frac{\arg E_k(t+\Delta t) - \arg E_k(t)}{\Delta t}. \tag{28}$$

This equation will be discussed in Appendix A. It is found that the electric field components with the constant phase velocity really exist, as is shown in Fig. 12. Further, the constant phase velocity is almost the same as the plateau region.

Actually, the SST is inaccurate to treat the long-time resonance problem, as is shown in Fig. 13. The test particle

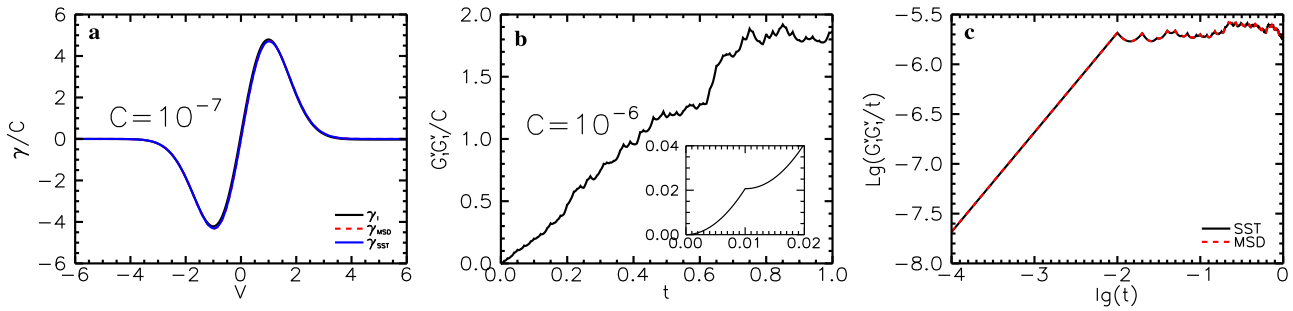

FIG. 7. (a) Flux in the velocity space in random field, which is normalized to C. Black line is the flux γ_I computed by integral; Red line is the flux γ_{MSD} is computed by the MSD; Blue line shows the flux γ_{SST} computed by the SST. (b) Time history of $\mathcal{G}_1^v\mathcal{G}_1^v$ at $v = 0$, which is normalized to C. (c) Time history of $\mathcal{G}_1^v\mathcal{G}_1^v/t$ at $v = 0$.

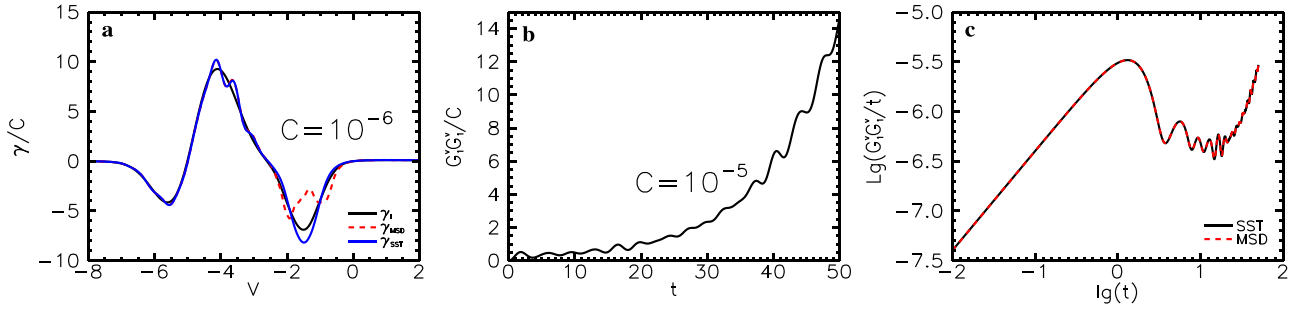

FIG. 8. (a) The quasilinear flux ($t \in [100, 150]$) in the BOT instability. Black line: the flux γ_I computed by the integral; Red line: the flux γ_{MSD} computed by the MSD; Blue line: the flux γ_{SST} computed by the SST. (b) Time history of $\mathcal{G}_1^v\mathcal{G}_1^v$ at $v=0$. (c) Time history of $\mathcal{G}_1^v\mathcal{G}_1^v/t$ at $v=0$.

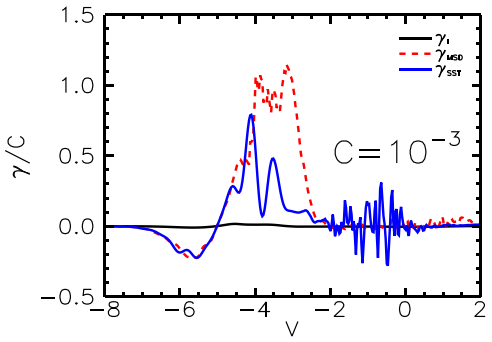

FIG. 9. The nonlinear flux ($t \in [250, 300]$) in the BOT instability. Black line: the flux γ_I computed by the integral; Red line: the flux γ_{MSD} computed by the ensemble averaged diffusion coefficient; Blue line: the flux γ_{SST} computed by the SST.

motion in a given electric potential ϕ_0 is computed by the SST.

$$\phi_0(x,t) = \delta\cos\left(k(x - v_0 t) - \omega t\right), \tag{29}$$

where $k=0.25$, $\omega=0.75$, $v_0=-5$. The phase velocity of the field is $\omega/k + v_0 = -2$. δ is chosen according to Figs. 6(b) and 6(d) to simulate the linear and the nonlinear stage. At the nonlinear stage, the amplitude of field is much larger than the one at the linear stage, so that the bounce time at the nonlinear stage is much shorter than that at the linear stage, which can also be seen from Figs. 13(c) and 14(c). The resonance problem is much important at the nonlinear stage. Unfortunately, the most part of the energy of the electric field at the nonlinear stage deposits in these components, and the perturbative method is going to collapse in a long time.

Therefore, neither the SST nor the conventional random-walk model (the flux γ_{MSD} shown in Fig. 9) can be used to describe the transport in the nonlinear stage of the

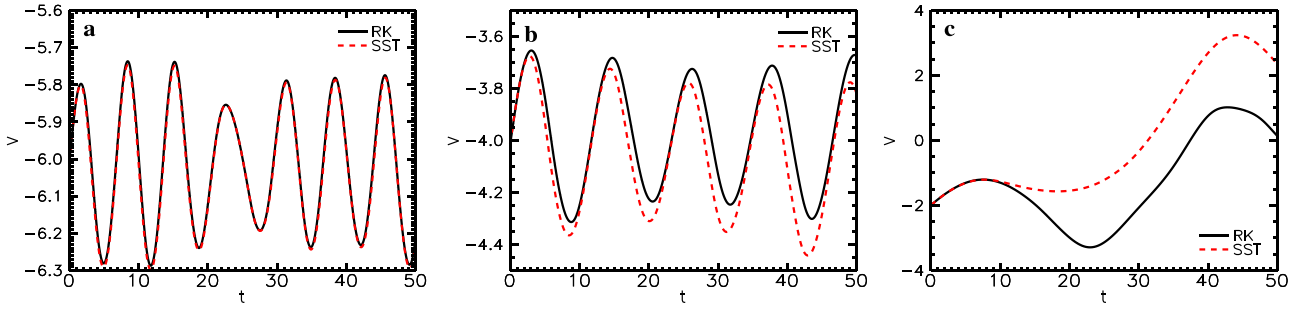

FIG. 10. Time history of particle velocity at the nonlinear stage. Red lines: the results of I-transform by the SST; Black lines: the results of the 2nd-order Runge-Kutta method.

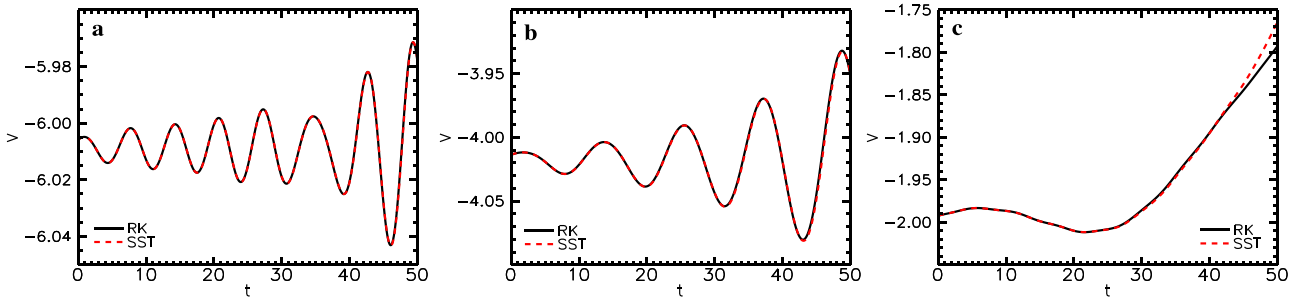

FIG. 11. Time history of particle velocity at the linear stage. Red lines: the results of I-transform by the SST; Black lines: the results of the 2nd-order Runge-Kutta method.

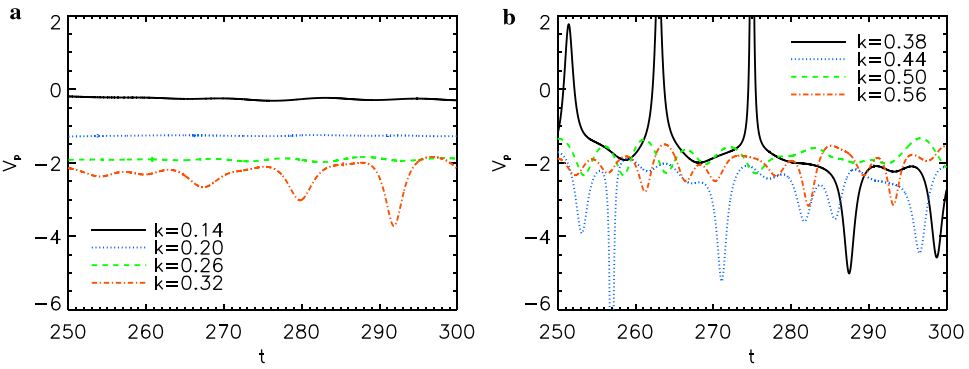

FIG. 12. The time history of phase velocities corresponding to different k.

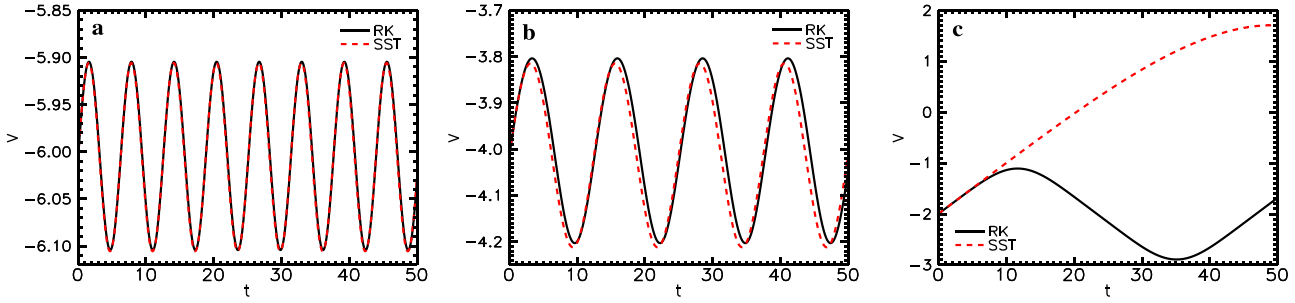

FIG. 13. The time history of particle velocity, with $\delta = 0.1$. Red lines: the results of I-transform by the SST; Black lines: the results of the 2nd-order Runge-Kutta method.

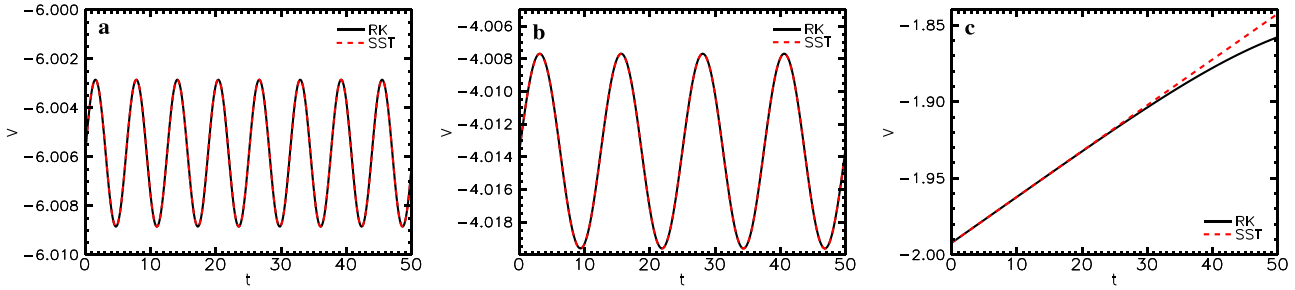

FIG. 14. The time history of particle velocity, with $\delta = 0.003$. Red lines: the results of I-transform by the SST; Black lines: the results of the 2nd-order Runge-Kutta method.

one dimensional Langmuir turbulence. The nonlinear transport cannot be well-described by a simple diffusion model, due to the strong particle trapping in the nonlinear stage.

V. SUMMARY AND DISCUSSIONS

In conclusion, a unified numerical approach, the I-transform approach based on the Lie-transform perturbation method, has been verified for the nonlinear kinetic simulation and transport analysis. The new approach evolves the perturbed system by using the evolution of the well-understood unperturbed system. For numerical cases, such as the Landau damping and the BOT instability, the results of the new approach agree with the well-established conservative semi-Lagrangian approach. For the accuracy of numerical simulation, the deviation between the perturbed and the unperturbed system should not be too large, the MST is used in simulation to avoid the large deviation. The information about the turbulence transport is involved in the generating vector fields computed by the SST. The transport properties of random walk model and the quasilinear transport are well-described by the turbulence scattering term, which can be explicitly computed by the SST. It is also found that the nonlinear transport in the one-dimensional Langmuir turbulence cannot be well-described by a simple random-walk model, due to the strong particle trapping in the nonlinear stage.

ACKNOWLEDGMENTS

This work was supported by the National Natural Science Foundation of China under Grant Nos. 11175178, 11375196, 11405174 and the National ITER program of China under Contract No. 2014GB113000.

APPENDIX A: NUMERICAL DIAGNOSIS OF THE PHASE VELOCITY

In this Appendix, Eq. (28) is discussed in detail. The electric field is defined in the laboratory coordinates $E = E(x, t)$. In the Fourier space, the coordinate transformation can simply be carried out by using

$$E(x,t)=\sum_k E_k(t)\mathrm{e}^{\mathrm{i}kx}=\sum_{k,\omega}E_{k,\omega}\mathrm{e}^{\mathrm{i}(kx-\omega t)}, \tag{A1}$$

we have

$$E_k(t)=\sum_\omega E_{k,\omega}\mathrm{e}^{-\mathrm{i}\omega t}. \tag{A2}$$

The explement of complex amplitude E_k can be computed by using

$$\arg(E_k)=\arctan\frac{\mathrm{Im}\,E_k}{\mathrm{Re}\,E_k}. \tag{A3}$$

Substituting Eq. (A2) into Eq. (A3), we have

$$\arg(E_k)=\arctan\frac{\mathrm{Im}\sum_\omega E_{k,\omega}\mathrm{e}^{-\mathrm{i}\omega t}}{\mathrm{Re}\sum_\omega E_{k,\omega}\mathrm{e}^{-\mathrm{i}\omega t}}=\arctan\frac{\sum_\omega |E_{k,\omega}|\sin(\theta_{k,\omega}-\omega t)}{\sum_\omega |E_{k,\omega}|\cos(\theta_{k,\omega}-\omega t)}, \tag{A4}$$

here the relation of $E_{k,\omega}=|E_{k,\omega}|\mathrm{e}^{\mathrm{i}\theta_{k,\omega}}$ is used.

If the electric field can be written as

$$E_k=E_{0;k}\mathrm{e}^{-\mathrm{i}\omega_0 t}+E_{1;k}\mathrm{e}^{-\mathrm{i}\omega_1 t}, \tag{A5}$$

with $\epsilon=|E_{1;k}|/|E_{0;k}|\ll 1$. To $\mathcal{O}(\epsilon)$,

$$\begin{aligned}V_p(k)&=-\frac{1}{k}\frac{\mathrm{d}}{\mathrm{d}t}\arctan\frac{|E_{0;k,\omega_0}|\sin(\theta_{k,\omega_0}-\omega_0 t)+|E_{1;k,\omega_1}|\sin(\theta_{k,\omega_1}-\omega_1 t)}{|E_{0;k,\omega_0}|\cos(\theta_{k,\omega_0}-\omega_0 t)+|E_{1;k,\omega_1}|\cos(\theta_{k,\omega_1}-\omega_1 t)}\\&=-\frac{1}{k}\frac{\mathrm{d}}{\mathrm{d}t}\arctan\frac{\sin(\theta_{k,\omega_0}-\omega_0 t)+\epsilon\sin(\theta_{k,\omega_1}-\omega_1 t)}{\cos(\theta_{k,\omega_0}-\omega_0 t)+\epsilon\cos(\theta_{k,\omega_1}-\omega_1 t)}\\&=-\frac{1}{k}\frac{\mathrm{d}}{\mathrm{d}t}\left(\theta_{k,\omega_0}-\omega_0 t+\epsilon\Phi(t)\right)\\&=\frac{\omega_0}{k}-\frac{\epsilon}{k}\frac{\mathrm{d}}{\mathrm{d}t}\Phi(t),\end{aligned} \tag{A6}$$

with $\Phi(t)=\sin(\theta_{k,\omega_1}-\omega_1 t)-\tan(\theta_{k,\omega_0}-\omega_0 t)\cos(\theta_{k,\omega_1}-\omega_1 t)$. It means that V_p oscillates around the phase velocity of the single frequency wave ω_0/k; If $E_{1;k}$ vanishes, V_p is exactly equal to the ω_0/k.

[1]A. A. Galeev and R. Z. Sagdeev, Sov. Phys. JETP-USSR **26**, 233 (1968); available at http://www.jetp.ac.ru/cgi-bin/e/index/e/26/1/p233?a=list.
[2]F. Hinton and R. Hazeltine, Rev. Mod. Phys. **48**, 239 (1976).
[3]R. Z. Sagdeev and A. A. Galeev, Dokl. Akad. Nauk SSSR **189**, 1204 (1969).
[4]R. Balescu, *Aspects of Anomalous Transport in Plasmas* (Institute of Physics Publishing, Bristol, 2005), Chap. 5–9, pp. 79–214.
[5]X. Garbet, Y. Idomura, L. Villard, and T. H. Watanabe, Nucl. Fusion **50**, 043002 (2010).
[6]W. M. Nevins, G. W. Hammett, A. M. Dimits, W. Dorland, and D. E. Shumaker, Phys. Plasmas **12**, 122305 (2005).
[7]W. Zhang, Z. Lin, and L. Chen, Phys. Rev. Lett. **101**, 095001 (2008).
[8]E. Sonnendrucker, J. Roche, P. Bertrand, and A. Ghizzo, J. Comput. Phys. **149**, 201 (1999).
[9]Y. Kominis, A. K. Ram, and K. Hizanidis, Phys. Rev. Lett. **104**, 235001 (2010).
[10]S. Wang, Phys. Plasmas **19**, 062504 (2012).
[11]S. Wang, Phys. Rev. E **87**, 063103 (2013).
[12]S. Wang, Phys. Plasmas **20**, 082312 (2013).
[13]Y. Xu, Z. Dai, and S. Wang, Phys. Plasmas **21**, 042505 (2014).
[14]S. Wang, Phys. Plasmas **21**, 072312 (2014).
[15]R. G. Littlejohn, J. Math. Phys. **23**, 742 (1982).
[16]A. Brizard and T. Hahm, Rev. Mod. Phys. **79**, 421 (2007).
[17]G. Manfredi, Phys. Rev. Lett. **79**, 2815 (1997).
[18]C. Z. Cheng and G. Knorr, J. Comput. Phys. **22**, 330 (1976).
[19]N. Crouseilles, M. Mehrenberger, and E. Sonnendrucker, J. Comput. Phys. **229**, 1927 (2010).
[20]J. Canosa, Phys. Fluids **17**, 2030 (1974).